JACS
JOURNAL OF THE AMERICAN CHEMICAL SOCIETY
Article
pubs.acs.org/JACS
Terms of Use

Synthesis of Tetragonal and Orthorhombic Polymorphs of Hf_3N_4 by High-Pressure Annealing of a Prestructured Nanocrystalline Precursor

Ashkan Salamat,*[,†,‡] Andrew L. Hector,*[,§] Benjamin M. Gray,[§] Simon A. J. Kimber,[‡] Pierre Bouvier,[∥] and Paul F. McMillan*[,⊥]

[†]Lyman Laboratory of Physics, Harvard University, Cambridge, Massachusetts 02138, United States
[‡]European Synchrotron Radiation Facility, BP 220, 38043 Grenoble Cedex, France
[§]Chemistry, University of Southampton, Southampton SO17 1BJ, United Kingdom
[∥]Laboratoire des Materiaux et du Genie Physique, CNRS, Université Grenoble-Alpes, 3 Parvis Louis Neel, 38016 Grenoble, France
[⊥]Department of Chemistry, Christopher Ingold Laboratory, University College London, London WC1H 0AJ, United Kingdom

ABSTRACT: Hf_3N_4 in nanocrystalline form is produced by solution phase reaction of $Hf(NEtMe)_4$ with ammonia followed by low-temperature pyrolysis in ammonia. Understanding of phase behavior in these systems is important because early transition-metal nitrides with the metal in maximum oxidation state are potential visible light photocatalysts. A combination of synchrotron powder X-ray diffraction and pair distribution function studies has been used to show this phase to have a tetragonally distorted fluorite structure with $^1/_3$ vacancies on the anion sites. Laser heating nanocrystalline Hf_3N_4 at 12 GPa and 1500 K in a diamond anvil cell results in its crystallization with the same structure type, an interesting example of prestructuring of the phase during preparation of the precursor compound. This metastable pathway could provide a route to other new polymorphs of metal nitrides and to nitrogen-rich phases where they do not currently exist. Importantly it leads to bulk formation of the material rather than surface conversion as often occurs in elemental combination reactions at high pressure. Laser heating at 2000 K at a higher pressure of 19 GPa results in a further new polymorph of Hf_3N_4 that adopts an anion deficient cottunite-type (orthorhombic) structure. The orthorhombic Hf_3N_4 phase is recoverable to ambient pressure and the tetragonal phase is at least partially recoverable.

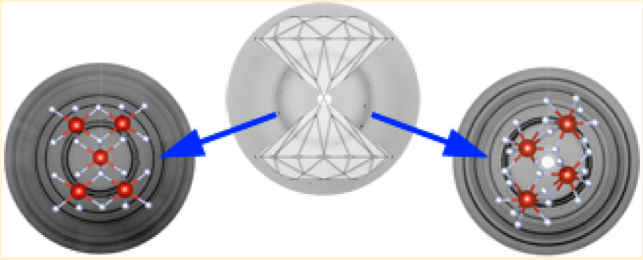

■ INTRODUCTION

One of the most obvious features of transition-metal nitride chemistry is that the maximum formal oxidation state of the metal is rarely as high as in the corresponding oxides or fluorides, e.g. TiN (Ti^{3+}) vs TiO_2 or Mo_5N_6 ($Mo^{3.6+}$) vs MoO_3.[1] These phases are typically metallic with strong orbital overlap between the metals and nitrogen in interstitial sites.[2] Hence like the carbides they find important applications as hard, refractory materials.[3] For some metals there are reports of higher formal oxidation states, and much of the interest in these compounds stems from the properties of Ta_3N_5. Currently Ta_3N_5 is the only known early transition-metal nitride phase with maximum oxidation state that is easy to prepare.[4] It is a bright orange-red, medium band gap semiconductor that has found applications as a pigment material.[5] It has also been heavily studied for visible light photocatalysis, notably by Domen who found a quantum efficiency of ∼10% for overall water splitting[6] and has recently examined its use to generate electrical currents in photoelectrochemical cells.[7]

Higher oxidation states are often found in defective versions of the more common phases, e.g., $Ti_{0.76}N$ single crystals with the rocksalt structure have been grown by the floating zone technique under gaseous N_2.[8] However, the characterization of distinct high oxidation state phases remains uncommon.[9] A red-brown, orthorhombic Eu_3O_4-type phase of Zr_3N_4, with face and corner linked ZrN_6 octahedra and trigonal prisms, can be prepared by high-temperature (1173 K) reaction of $ZrCl_4$ with NH_3.[10] Laser-heated diamond anvil cells (LH-DACs) have been used to produce a number of significant main group nitride phases,[11] and Zerr et al. demonstrated their potential for formation of new nitrogen-rich transition-metal nitride phases.[12] They made cubic (Th_3P_4-type) phases of Zr_3N_4 and Hf_3N_4, with face-linked ZrN_8 distorted cubes, using elemental combination reactions at 15.6−18 GPa and around 3000 K. These phases are narrow band gap semiconductors that can be recovered to ambient pressure and are hard materials with a bulk modulus of K_0 = 227(7) GPa for c-Hf_3N_4.[13] A series of platinum metal nitrides, such as PtN_2, IrN_2, and OsN_2, have since been made under these conditions,[14,15] but other nitrogen-rich early transition-metal nitrides have remained elusive.

Received: April 4, 2013
Published: May 30, 2013

 © 2013 American Chemical Society

"Soft" synthesis routes that avoid the high temperatures and long annealing times typically used in solid-state preparations have produced a number of important groups of materials. These include the crystallization of aluminosilicate gels around molecular templates to make zeolites[16] and topotactic transformations leading to surprising crystal structure elements, such as the sheets of FeO_4 square planes in $SrFeO_2$.[17] There are a small number of such examples in nitride chemistry such as the intercalation of Li into ZrNCl to make the superconducting Li_xZrNCl phase[18] and nitrogen cycling in the $Co_3Mo_3N \leftrightarrow Co_6Mo_6N$ catalytic system.[19] The development of "soft" routes to new metal nitride phases with high nitrogen contents offers the possibility of obtaining metastable phases that cannot be obtained from solid-state reactions.

Most precursor-based metal nitride synthesis yields similar materials to those obtained at high temperature (often rocksalt-type MN), but Baxter et al. showed that solution phase ammonolysis of metal amides followed by firing often results in an intermediate temperature plateau in the mass loss profile corresponding to the M_3N_4 composition (M = Ti, Zr, Hf, V, Nb).[20] There is evidence of the local structure in the precursor influencing that of the final product in the observation of a rocksalt-like structure by X-ray absorption spectroscopy in an amorphous carbonitride material close in composition to Ti_3N_4 prepared in this way.[21] Similarly there are examples of the reactions of amides with ammonia resulting in unexpected results in chemical vapor deposition (CVD) of thin films. Most relevant here is the work of Fix et al., who obtained Zr_3N_4 and Hf_3N_4 from $M(NEt_2)_4$ (M = Zr and Hf) complexes and ammonia.[22] These phases had broad diffraction patterns closely resembling rocksalt but with an increase in lattice parameter compared with ZrN or HfN and a possible rhombohedral distortion that was suggested to be due to the filling of tetrahedral anion sites. An apparently similar bulk material has been prepared by Li et al. from reactions of $M(NEt_2)_4$ (M = Zr and Hf) with ammonia.[23] Like the CVD-derived materials these were found to have diffraction patterns closely resembling rocksalt, with very broad reflections and a displacement of some peaks that was also suggested to be due to a rhombohedral distortion. We will refer to this and a similar material made by ourselves as "nanocrystalline Hf_3N_4".

The combination of a preformed precursor with high-pressure treatment is an attractive option for synthesis of nitrogen-rich phases as it offers the possibility of stabilizing the higher oxidation state to higher temperature to allow crystallization. Annealing the nanocrystalline Zr_3N_4 and Hf_3N_4 materials discussed above in a multianvil press at 12 GPa and 1873 K produced an oxynitride for the zirconium reaction with the Th_3P_4 structure type as found for the pure nitride but with a small increase in lattice parameter. In the analogous hafnium reaction only the Th_3P_4-type c-Hf_3N_4 was produced with traces of hafnium oxide and oxynitride.[24] Diamond anvil cells (DACs) offer a well-contained environment and also the possibility of increasing the nitrogen activity by preloading with nitrogen at high pressure so are ideal for controlled crystallization or phase transformation in these metal nitrides. In this study we have crystallized amide-derived nanocrystalline Hf_3N_4 samples in DACs at 12 GPa and 1500 K to produce a defect fluorite-related tetragonal polymorph and shown that the material prior to crystallization also has a similar tetragonal fluorite structure rather than the previously proposed rocksalt-like structure. By heating to 2000 K at 19 GPa for 240 s it has also been possible to obtain a defect cottunite-related orthorhombic polymorph. The combination of precursor-based synthesis and high-pressure crystallization could be very productive in synthesis of nitrogen-rich metal nitride phases.

■ RESULTS AND DISCUSSION

The synthesis of nanocrystalline Hf_3N_4 was achieved by exposing a solution of $Hf(NEtMe)_4$ to a large excess of dry liquid ammonia to precipitate a polymeric material of likely composition $[Hf(NH)_x(NH_2)_y(NEtMe)_z]_n$ and heating this polymer in ammonia at 673 K. The bright-orange product closely resembles that obtained by Li et al.[23] from reactions of $Hf(NEt_2)_4$ with flowing ammonia in a furnace tube, but precipitation from solution would facilitate its synthesis on a much larger scale. Combustion microanalysis confirmed the composition as Hf_3N_4, with small residual amounts of H from the precursor. The sample was handled and measured only in a carefully controlled inert atmosphere (argon or nitrogen) glovebox to prevent contamination with oxygen and was reanalyzed after the work was complete.

The bright-orange color of nanocrystalline Hf_3N_4 is particularly significant considering the pigment applications and photocatalytic activity of Ta_3N_5. Examination of the UV–vis absorption spectrum (Figure 1) shows that the band edge is actually only slightly higher in energy than that of HfO_2 (~270 vs ~230 nm), as expected from the lower electronegativity of nitrogen compared with oxygen (reducing the band gap). The color is due to a broad transition centered at around 350 nm. Since the metal ions present are Hf^{4+} (d^0) this is assumed to be a ligand-to-metal charge transfer band.

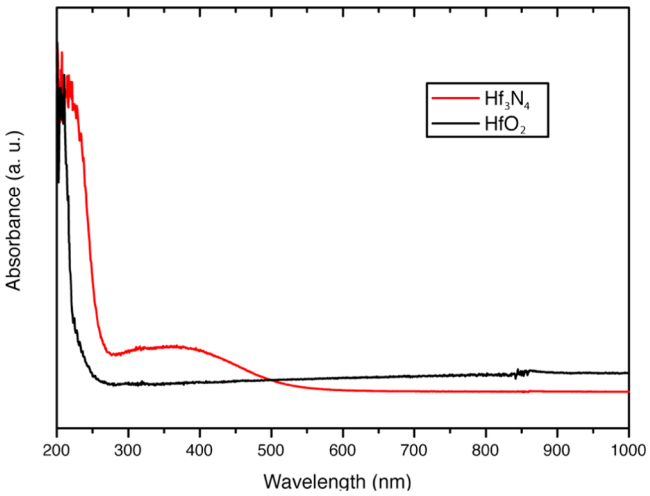

Figure 1. Diffuse reflectance spectra (diluted in $BaSO_4$) of nanocrystalline Hf_3N_4 (top) and HfO_2 (bottom).

The broad X-ray diffraction (XRD) pattern of nanocrystalline Hf_3N_4 closely resembled a face-centered cubic lattice but with similar variations in peak positions to those previously attributed by others to a rhombohedral distortion,[22,23] most notably too large a separation between the first two reflections that would be indexed as the 111 and 200 reflections of rocksalt. Le Bail refinement, which ignores the atom positions and simply refines intensities on each reflection, resulted in a reasonable fit in $R\bar{3}m$ with a = 4.608 Å and α = 87.81°. However, Rietveld refinement always resulted in too much intensity on the 200/002 reflection, and no structure model could be found that gave a good fit. In our study we revisited

this structure refinement after we had observed crystallization of the material at high pressure and temperature. This will be discussed further after that crystallization is described.

Structure of Tetragonal (*I*4/*m*) Hf_3N_4 Obtained at 12 GPa and 1500 K. *In situ* high-pressure annealing experiments used a CO_2 laser source to heat the sample in a nitrogen-filled DAC, while synchrotron XRD data were used to monitor the degree of crystallization. Sample loading was carried out under carefully controlled inert conditions (H_2O and O_2 <1 ppm). Initially nanocrystalline Hf_3N_4 was compressed to 12 GPa (Th_3P_4-type Hf_3N_4 was predicted to be stable above 9 GPa),[25] and the broad, diffuse rings due to nanocrystalline Hf_3N_4 remained apparent in the XRD pattern. On laser heating at the lowest power setting where a thermal glow was observed (1500 K), sharp textured rings appeared almost immediately (Figure 2). Heating was continued for ∼90 s although no further change was observed after ∼60 s.

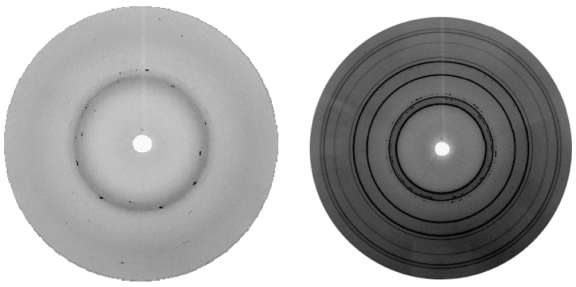

Figure 2. Diffraction plate image of nanocrystalline Hf_3N_4 at 12 GPa before laser heating (left) and crystallized tetragonal Hf_3N_4 after laser heating for 60 s (right). The heavily textured diffraction rings in both images are due to the nitrogen pressure transmitting medium/thermal insulator; these were removed by masking when the images were integrated.

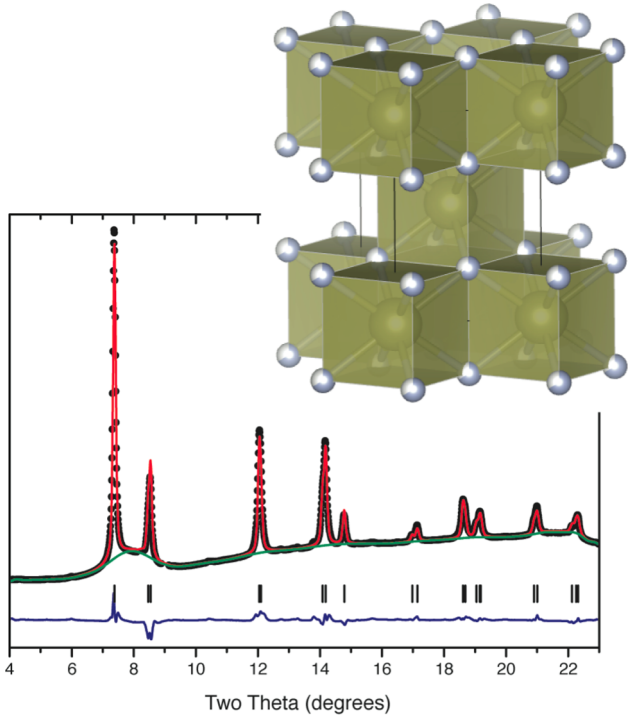

Figure 3. Fit to the XRD pattern of Hf_3N_4 obtained at 12 GPa and 1500 K using a tetragonally distorted anion-defective fluorite model (R_{wp} = 2.2% and R_p = 2.0%). The data points are shown as black dots and the Rietveld fit as a red line. The refined background is shown in green and the difference plot in blue. Tick marks represent the allowed reflection positions in *I*4/*m*. The structure (inset) consists of edge-linked HfN_8 cubes with a small tetragonal distortion; note that due to the $^1/_3$ nitrogen vacancies the average Hf coordination number is 5.33.

A small fraction of the sample remained uncrystallized as the broad features due to nanocrystalline Hf_3N_4 remained in the powder XRD under the sharp reflections (Figure 3 between 7 and 9°). This small amount of unconverted nanocrystalline precursor in the tetragonal phase could be a consequence of insulator efficiency or temperature gradients due to the diamonds or the use of single-sided CO_2 laser heating. However, this impurity level is much smaller than that observed in elemental combination reactions, where typically only the surface of the sample is reacted and a large quantity of metal or lower nitride phases is found in the products.[14,15]

The XRD pattern of Hf_3N_4 after annealing closely resembled a face-centered cubic cell, but a number of small peak splittings were obvious. This pattern clearly did not match the known Th_3P_4-type phase of Hf_3N_4 that has been calculated to be stable at pressures above 9 GPa.[25] Initial efforts focused on trying to fit these to a rhombohedrally distorted rocksalt cell as previously suggested for nanocrystalline Hf_3N_4.[22,23] However, none of these attempted solutions were successful. Close inspection of the peak splitting pattern pointed to a tetragonal distortion of the face-centered cubic lattice, but this distortion with rocksalt-derived atom positions was also unsuccessful in fitting the observed intensities. The rocksalt and fluorite structures are both based on cubic close-packed arrays of metal atoms that dominate the diffraction signal, but the anions occupy octahedral sites in the first instance and tetrahedral holes in the second case. We obtained a good Rietveld fit using a tetragonally distorted defective fluorite-type structure in space group *I*4/*m*, with a = 3.547(4) and c = 5.064(5) Å (Figure 3). Hf atoms occupy Wyckoff sites 2a (0,0,0) with N atoms and vacancies at 4d (0,0.5,0.25). Due to the limited scattering ability of the light N atoms, the site occupancy and the average isotropic thermal parameter for the anion sites were set at a fixed value for the refinement.

The tetragonal diffraction pattern remained single phase during decompression down to a pressure of 6.5 GPa. Below 6.5 GPa the membrane-driven DAC lost pressure with a sudden jump to ambient pressure in the sample, and a repeat experiment with the same cell suffered the same problem. Extra reflections were observed in the diffraction patterns of the recovered samples at ambient pressure. Hence, while these recovered samples contained the tetragonal Hf_3N_4 phase, further work will be necessary to clarify whether it can be recovered as a single phase following a slower stepwise decompression.

The 1500 K synthesis temperature is higher than the likely ambient pressure decomposition temperature of Hf_3N_4 based on the behavior of related phases, e.g., Ta_3N_5 loses nitrogen at around 1200 K. Our synthesis approach uses preformed nanocrystalline Hf_3N_4 and so does not require nitridation. This is important as the high bond energy of the N≡N molecule makes synthesis of higher nitrides from the elements problematic.[9] However, loading DACs with nitrogen at high pressure not only acts as a pressure transmitting medium and thermal insulator but also results in an increase in the nitrogen activity during heating in the closed system.[26] This may or may

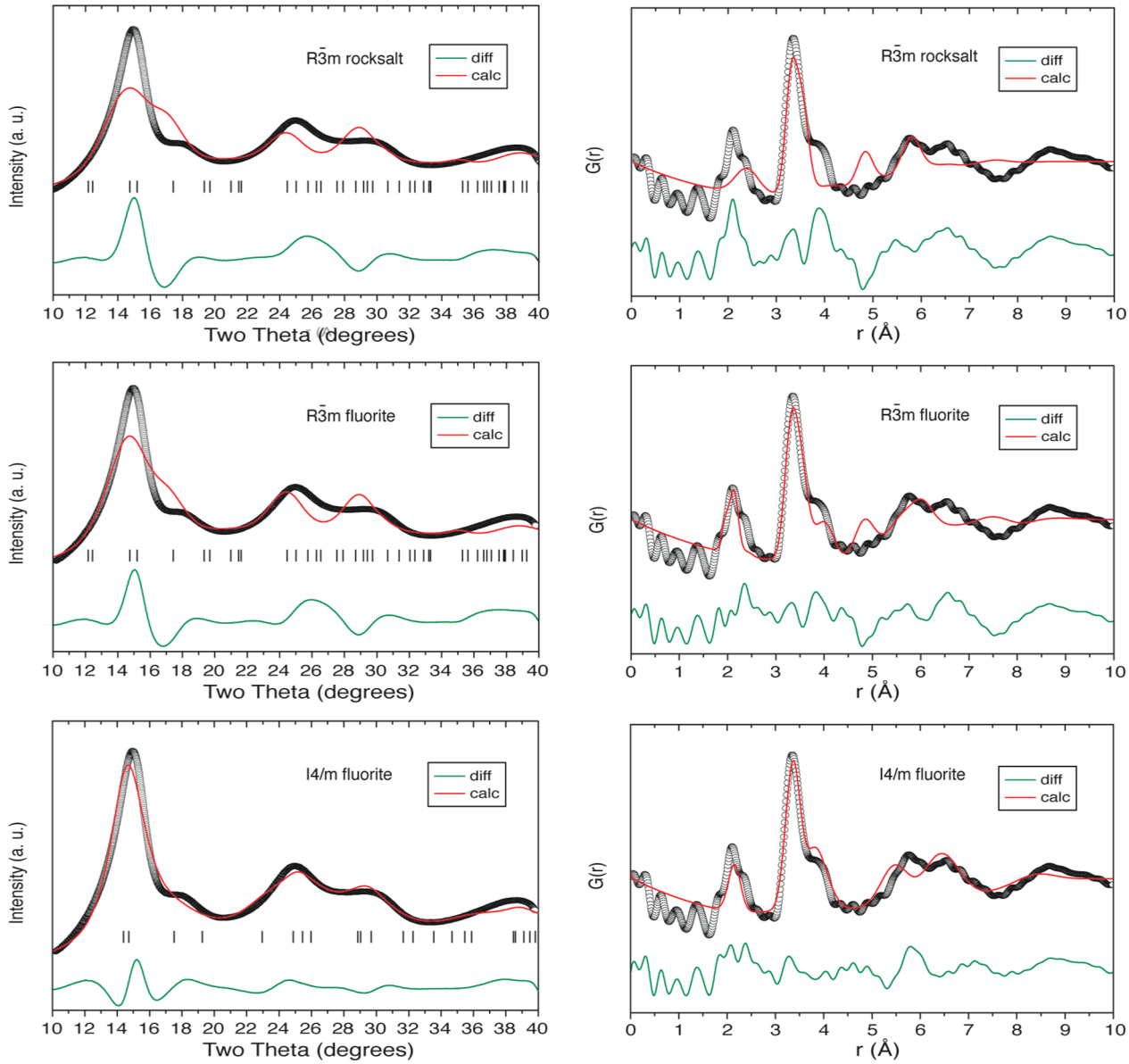

Figure 4. Rietveld (λ = 0.69775 Å) (left) and PDF (λ = 0.13788 Å) (right) fits to the diffraction data collected with nanocrystalline Hf_3N_4. The models used in fitting were rhombohedrally distorted rocksalt (top: Rietveld a = 4.491(3)Å, α = 88.578(4)°, R_{wp} = 21.4%, R_p= 20.5%; PDF a = 4.95913 Å, α = 85.3194°, R_p= 56.6%), rhombohedrally distorted fluorite (middle: Rietveld a = 4.607(4) Å, α = 88.706(3)°, R_{wp} = 15.6%, R_p= 12.5%; PDF a = 4.8646 Å, α = 92.4758°, R_p= 39.9%), and tetragonally distorted fluorite (bottom: Rietveld a = 3.152(1) Å, c = 5.220(7) Å, R_{wp} = 9.5%, R_p= 8.0%; PDF a = 3.2513 Å, c = 4.9845 Å, R_p= 32.0%).

not be important in stabilizing Hf_3N_4 during the crystallization process.

Structure of Nanocrystalline Hf_3N_4 Revisited. In the context of the tetragonal structure solution described above, the structure of the nanocrystalline Hf_3N_4 starting material was re-examined. Previous authors and our Le Bail fitting had supported a rhombohedral distortion, but the peak intensity distribution in Rietveld fitting did not support this model. A number of possible structure models were trialled including rocksalt and fluorite, and both with a rhombohedral or a tetragonal distortion. The best three fits are shown in Figure 4. As mentioned previously the cubic models produce the wrong spacing between Bragg peak positions. Both rhombohedral and tetragonal distortions can provide an improvement in the peak positions and a better Le Bail fit. However, a rocksalt-like arrangement of atoms did not provide a reasonable Rietveld fit with either distortion. Better solutions were obtained with fluorite-derived structures, and the statistically best fit is the tetragonally distorted ($I4/m$) fluorite cell that is also observed after crystallization at 12 GPa and 1500 K. This is an interesting result, in that it indicates that Hf_3N_4 adopts a tetrahedral site location for the N atoms within a cubic close-packed metal arrangement, rather than the octahedral holes occupied by anions in the rocksalt-based interstitial nitrides with smaller cations including "Ti_3N_4".[21]

Due to concerns that Rietveld fitting might not yield a unique solution with such broad reflections a pair distribution function (PDF) analysis was also undertaken, and the data fitted to the same set of models. The same three models yielded the best fits (Figure 4). Rocksalt-type models fail to fit the first shell at around 2 Å. While the rhombohedrally distorted fluorite structure provides a better fit, the first shell is slightly short in

the best fit that could be obtained, the intensity ratio between the first two shells is wrong, and the fit to the shoulder in the PDF at around 4 Å is poor. These features are all fitted well with the tetragonal fluorite model.

The observation that nanocrystalline Hf_3N_4 is isostructural with the phase obtained by laser annealing at 12 GPa is highly significant as it suggests that at this moderate pressure with a short period of high-temperature annealing, the structure has not changed. These conditions are within the predicted stability range of Th_3P_4-type Hf_3N_4.[25] The crystallite size has increased significantly, so the existing nanocrystals have acted as nuclei for the growth of the new tetragonal Hf_3N_4 polymorph. The structure has been determined either during formation of the polymeric precursor or during its low-temperature (673 K) decomposition to nanocrystalline Hf_3N_4. It is likely that the tetragonal distortion of the unit cell is related to the presence of the 33% vacancies on the tetrahedrally bonded N sites. These may be statistically distributed or have some local order. It is possible that the small deviations between the structural model and the experimental PDF data at longer distances are due to defect site ordering, some limited occupation of octahedral anion sites, or "amorphous" contributions from the surfaces of the nanocrystals.

Small differences in lattice parameters are observed in the PDF fits relative to the Rietveld fits due to uncertainties associated with the broad data from this nanocrystalline material. However, a larger difference is observed between the average molar volume of nanocrystalline Hf_3N_4 (28.4 $Å^3$ PDF or 26.8 $Å^3$ Rietveld per $HfN_{1.33}$ unit) and that of the crystallized tetragonal Hf_3N_4 (31.9 $Å^3$). Lattice parameter reductions with smaller particle size in nanoparticles are common. In metals this is ascribed to the balance between surface energy and the elastic properties of the material.[27] At small sizes the effect of surface energy is increased, and this results in a compression of the particle volume. Similar effects have been used to explain a reduction in cell parameter in small particles of CeO_2,[28] and we previously reported similar lattice parameter changes in TiN.[21]

An anion-defective cottunite-type structure (*Pnma*) as described in the next section was also tested, but the tetragonal fluorite structure yielded better fit statistics in both Rietveld and PDF fitting.

Structure of Orthorhombic (*Pnma*) Hf_3N_4 Obtained at 19 GPa and 2000 K. Heating nanocrystalline Hf_3N_4 at 19 GPa for 240 s at 2000 K resulted in a distinctly more complex diffraction pattern. This was indexed with an orthorhombic unit cell. The similarity of this unit cell shape with that of cottunite-type HfO_2 (a = 5.55, b = 3.30 and c = 6.48 Å with space group *Pnma*)[29] was noted, and hence structure refinement used this as a model structure. Refinement proceeded smoothly to give a good fit with a = 5.588(5), b = 3.317(1) and c = 6.475(6) Å (Figure 5). The Hf atoms occupy Wyckoff site 4a (0.259(2), 0.25, 0.385(1)) and N atoms two 4e sites (0.109(5), 0.25, 0.102(3) and −0.013(4), 0.75, 0.640(4)). As with the tetragonal phase this structure is anion deficient with both nitrogen sites at $^2/_3$ occupancy, and similarly the occupancies and thermal parameters of the N sites were not refined.

Orthorhombic Hf_3N_4 is fully recoverable to ambient pressure conditions. Attempts at synthesis at higher pressure also confirmed that this phase is stable up to at least 50 GPa without further phase change. The Th_3P_4-type phase of Hf_3N_4 was synthesized from the elements at a similar pressure (18 GPa) but at a significantly higher temperature (3000 K).[12] It is not clear whether the new orthorhombic phase forms due to a topotactic change from tetragonal Hf_3N_4 in these relatively short time scale reactions or due to thermodynamic stability under these temperature/pressure conditions. However, the conversion of fluorite-type materials to cottunite-type ones at high pressure (often via the orthoI phase) is common.[30]

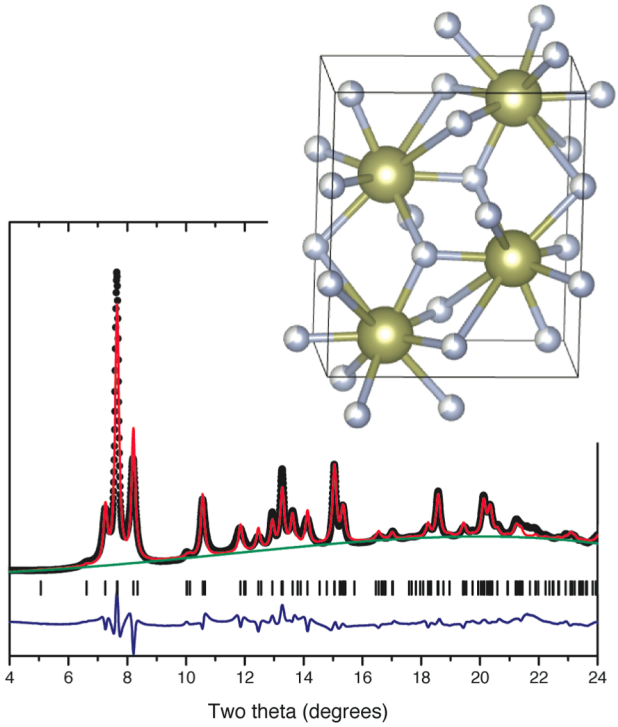

Figure 5. Rietveld fit (R_{wp} = 4.2% and R_p = 2.9%) to the XRD pattern of Hf_3N_4 at 19 GPa after laser heating at 2000 K for 60 s using a defect cottunite structure model. The data points and Rietveld fit are overlaid in black dots and a red line, respectively. The refined background is shown in green and the difference plot in blue. The refined structure (inset) has edge- and face-sharing HfN_9 tricapped trigonal prisms. Note that due to the $^1/_3$ nitrogen vacancies the average coordination number of the Hf atoms is 6.

Raman Spectra of Nanocrystalline and LH-DAC Annealed Hf_3N_4 Samples. The Raman signature of nanocrystalline Hf_3N_4 showed no prominent bands other than a broad feature at around 150−200 cm^{-1} superimposed on a rising fluorescence background (Figure 6). This is typical of materials that are commonly termed "amorphous", and it indicates the presence of substantial structural disorder and/or vacancy distribution within an otherwise crystalline sublattice due to the disappearance of q = 0 selection rules for phonon propagation. It is also reminiscent of the spectra of slightly anion-deficient transition-metal mononitrides, including ZrN, HfN, and NbN that have a one-phonon density of states characterized by two bands below 200 cm^{-1} due to transverse and longitudinal accoustic phonon branches and a high-frequency (500−600 cm^{-1}) band due to metal−nitrogen stretching.[29]

Unexpectedly the extreme broadening of the Raman spectrum observed in nanocrystalline Hf_3N_4 persisted even after crystallization of the tetragonal phase. That result can only mean that although the XRD signal reveals significant ordering mainly within the metal sublattice, phonon propagation is just as severely hampered as within nanocrystalline Hf_3N_4. We note that rocksalt-structured materials have no allowed first-order

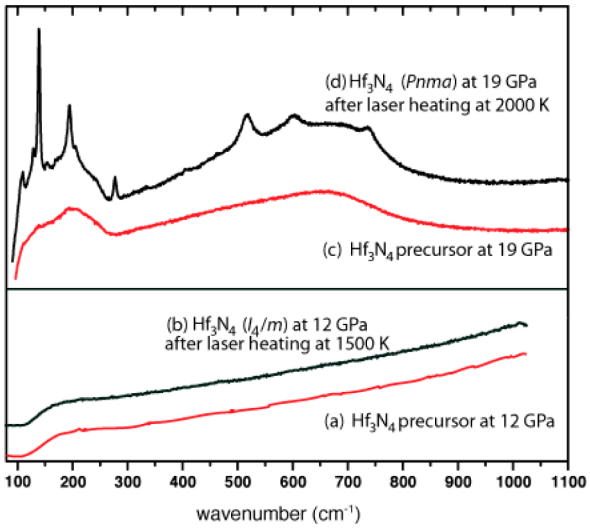

Figure 6. Raman spectra of Hf_3N_4 in N_2 pressure transmitting medium taken at (a) 12 GPa at ambient *T* before heating; (b) 12 GPa at ambient *T* after laser heating at 1500 K for 90 s; (c) 19 GPa at ambient *T* before heating; and (d) 19 GPa after laser heating at 2000 K for 60 s.

Raman bands, and crystalline fluorite has a single triply degenerate peak at the Brillouin zone center so we should not expect any rich Raman spectrum for these phases. The main Raman feature developed in both the starting material and that compressed and heated at 12 GPa is a broad maximum at around 200 cm^{-1}, corresponding to the acoustic density of states with main contributions from the heavy atoms. Although the diffraction results indicate macroscopic crystallization of the sample based on a reorganization of the Hf^{4+} positions, the Raman spectrum shows that the anion and vacancy site distributions do not permit full phonon propagation. Similar effects are observed for related systems, including anion-deficient cubic zirconia.[31]

After laser heating to 2000 K at 19 GPa, a series of sharp peaks appears in the Raman spectrum indicating formation of the high-pressure crystalline phase. XRD indicates formation of an anion-deficient cottunite structure. The sharp features at very low wavenumber (under 150 cm^{-1}) are similar to those observed for HfO_2. This is expected because these modes are due to vibrations of the heavy Hf^{4+} cations that occupy all of the available sites. The higher frequency vibrations are Hf−N stretching modes, but they are all shifted to lower frequency when compared to cottunite-type HfO_2. These modes are also broadened, presumably due to some disordering in the anion vacancy positions. This suggests that the broadening has a common origin in anharmonicity of the light element stretching vibrations that might be associated with electron−phonon coupling effects.[26]

The background to the Raman spectrum of crystallized orthorhombic Hf_3N_4 is similar to the profile observed for the compressed precursor material before laser heating (Figure 6). This raises the possibility that some change occurs in the nanocrystalline Hf_3N_4 during pressurization. The other possibilities are that the synthesis conditions are above the pressure required for a defect fluorite to defect cottunite phase transition (in which case this transition could have occurred in the nanocrystalline material) or that the sample is only partially crystallized during the laser heating experiment.

Compressibility of the New Hf_3N_4 Phases. The compressibility of the tetragonal and orthorhombic Hf_3N_4 phases were determined during decompression following synthesis at pressures of 12 and 19 GPa, respectively. Plots of the unit cell volumes are given in Figure 7, and these were fitted

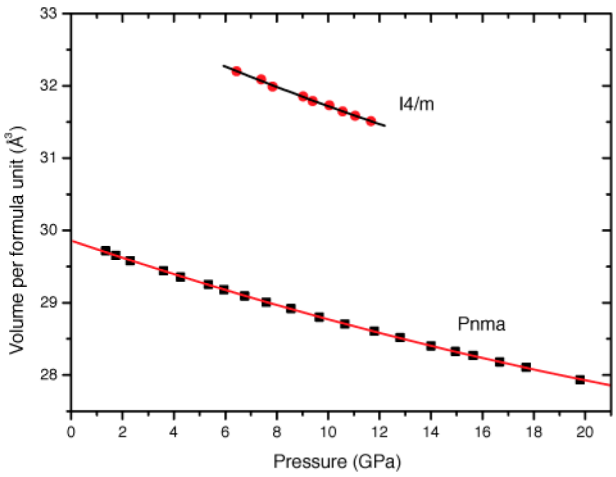

Figure 7. Volume−pressure relationships per $HfN_{1.33}$ formula unit of the tetragonal ($I4/m$) and orthorhombic (*Pnma*) phases of Hf_3N_4 during decompression following laser heating. Both phases are fitted to a third-order Birch−Murnaghan equation of state (fit lines).

to third-order Birch−Murnaghan equation of state relationships to determine the compressibility of the new Hf_3N_4 structures. The bulk modulus (K_0) and its pressure derivative (K') are determined for each phase using an extrapolated volume (V_0) at ambient pressure. For the tetragonal ($I4/m$) phase the fitted parameters were K_0 = 200(10) GPa and K' = 3.8(3), with V_0 = 66.32 Å^3. As expected for such anion-deficient structures, these values indicate a more compressible material than Th_3P_4-structured c-Hf_3N_4 (K_0 = 227(7) GPa with K' = 5.3(6))[12] or the tetragonally distorted fluorite-type HfO_2 with full anion occupancy (K_0 = 220 GPa).[32] Stepwise decompression of the orthorhombic Hf_3N_4 phase results in a smooth volume change (Figure 6) with K_0 = 279(16) GPa, K' = 2.41(9), and V_0 extrapolated to 119.3 Å^3. Significantly this defective material has a much larger bulk modulus than the Th_3P_4-structured c-Hf_3N_4 described above and synthesized at a similar pressure. In fact this seems a common feature among the oxides where the cotunnite structure has the highest coordination number possible for a MO_2 species and therefore the most incompressible structure type attainable.[27] However, as expected from the defect structure the cotunnite (*Pnma*) Hf_3N_4 is still significantly more compressible than the super hard, highly incompressible cotunnite (*Pnma*) HfO_2 phase with K_0 = 312−340 GPa.[31,33,34]

Comparison of the New Hf_3N_4 Phases with Those of HfO_2. We note that both the tetragonal and orthorhombic Hf_3N_4 phases are anion-defective analogues of high-pressure HfO_2 phases. Hence it is important to consider whether the phases described above could result from oxidation of nanocrystalline Hf_3N_4.

Crucially there is no evidence for formation of oxide species in the 12 GPa Raman spectra of the nanocrystalline or crystallized tetragonal Hf_3N_4 phases. HfO_2 phases have intense Raman active modes in the 100−700 cm^{-1} region,[35] and we would expect Hf oxynitrides to exhibit similar features based on data for ZrO_xN_y and TaON.[36] The lack of any observable modes in this range shows that any oxygen incorporation must

be minor and disordered. In a previous synthesis of Th_3P_4-type Hf_3N_4 in a multianvil press the presence of oxide led to segregation of oxide and oxynitride phases but without detectable formation of $Hf_3(N,O)_4$ solid solution.[24] That behavior contrasts with the Zr system where $Zr_{2.86}(N_{0.88}O_{0.12})_4$ was formed. The Raman spectrum of orthorhombic Hf_3N_4 obtained here is related to that obtained for cottunite-type HfO_2 in the same pressure range.[34,35,37] The low-energy peaks that are related to the metal sublattice have similar values, but the higher frequency Hf−N modes are all shifted to lower frequency.

At high temperature and ambient pressure, HfO_2 exhibits three polymorphs. The ambient temperature monoclinic structure ($P2_1/c$) transforms above 1400 K to a tetragonal structure[38] ($P4_2/nmc$) that is stable to 2640 K. This is followed by a cubic fluorite structure (space group $Fm\bar{3}m$). Room temperature compression first yields the ortho I ($Pbca$) phase before the high-pressure cottunite phase ($Pnma$) forms sluggishly above 30 GPa.[32] Tang et al. later showed that at 773−973 K the ortho I to cottunite phase transition can be achieved at 14 GPa.[39] The tetragonal fluorite modification of HfO_2 ($P4_2/nmc$) forms at high pressure and high temperature. Its stability as described by Ohtaka et al.[32] begins at 1700 K and follows a negative boundary slope to a minimum of 1200 K at 4 GPa. This extends to 1400 K and 14 GPa before transformation into the stable high-pressure cottunite-type phase. Unsurprisingly the conditions for this transformation do resemble the conditions in which the defect cottunite-type phase of Hf_3N_4 forms from the tetragonal fluorite modification. However, as noted in the previous section the compressibility data are consistent with defective structures for Hf_3N_4.

■ CONCLUSIONS

Low-temperature pyrolysis of the polymer formed by solution phase reaction of $Hf(NEtMe)_4$ results in an anion defective tetragonal fluorite structure. High-pressure laser annealing of this material under relatively gentle conditions (relative to elemental combination at high pressure) results in crystallization of the same structure. This is possible because of the containment offered by diamond anvil cells. Short heating times may also be important. At higher pressure and temperature an orthorhombic, defect cottunite-type Hf_3N_4 polymorph is obtained from the same nanocrystalline precursor. Both the tetragonal and orthorhombic phases are anion-defective analogues of known high-pressure HfO_2 phases, but Raman spectroscopy demonstrates that the new phases do not contain significant quantities of oxide. They are also more compressible than the oxide analogues due to their defective structures. High pressure crystallization and transformation of precursor-derived materials represents an important step forward in synthesis of nitrogen-rich metal nitrides as the entire sample can be converted and is likely to be applicable to the discovery of new nitride phases containing other metals.

■ EXPERIMENTAL TECHNIQUES

Tetrahydrofuran (THF) was distilled from sodium/benzophenone ketyl ether and stored under nitrogen. Ammonia was distilled from a sodium/liquid ammonia solution and stored in a stainless steel pressure can. $Hf(NEtMe)_4$ was provided by SAFC Hitech and used as received. $Hf(NEtMe)_4$ (2 cm^3) was dissolved in THF (20 cm^3) and cooled to −78 °C. Dry ammonia (20 cm^3) was condensed into this solution and then allowed to warm slowly to room temperature. The solvent was removed *in vacuo* to leave a white powder. This powder was heated in dry flowing ammonia to 400 °C at a ramp rate of 1 °C min^{-1}, and the temperature was maintained for 20 min before allowing to cool naturally. The orange product was then crushed to a powder.

Powder XRD (Bruker D8 with GADDS diffractometer, Cu-$K_{\alpha 1}$) yielded patterns closely resembling the "rhombohedrally distorted rocksalt" phase previously reported by Li et al.[23] Combustion microanalysis (outsourced to Medac Ltd.) gave a composition of C 0.24%, H 0.68%, and N 9.45% (theory N = 9.47% based on Hf_3N_4; the carbon content is below the ±0.3 wt % error limit of the technique).[14] UV−vis spectra were recorded in diffuse reflectance geometry using a Perkin-Elmer Lambda 35 spectrometer with integrating sphere.

High-pressure experiments were carried out using diamond anvil cells with culet sizes of 600 or 300 μm for maximum pressures of 15 and 50 GPa, respectively. Re gaskets were drilled using a Nd:YAG laser. Angle dispersive XRD was conducted at the European Synchrotron Radiation Facility at the Swiss-Norwegian beamline (SNBL) and the high-pressure beamline ID27 using monochromatic X-rays with λ = 0.69775 and 0.3738 Å, respectively. All loadings were carried out in an argon glovebox. High-pressure crystallization was carried out on samples loaded in a glovebox, elevated from the diamond surfaces using a tripod of ruby fragments. The DAC was then sealed shut and placed in a Sanchez Tech gas loading system, and after purging the DAC was then reopened by imposing a negative difference in pressure. We have developed this technique with a number of very sensitive systems and are thus confident that the sample is not exposed to air during the process.[40] Nitrogen was then pumped at 1400 bar serving as a thermal insulator and pressure transmitting medium, and the cell was closed at 0.2 GPa. All laser heating experiments were conducted at ID27 using the online CO_2 (λ = 10.6 μm) laser heating system. Temperature measurements were calculated during laser heating by collecting emission spectra in reflective geometry and fitting to a Planck function. Data were collected using either a MarCCD 165 or MAR345 detector with 60 s exposure times. Rietveld refinements employed the GSAS package.[41]

Pair distribution functions were calculated from powder diffraction profiles collected at ID15B (90 KeV X-rays and data acquired with a Mar345 detector) using in-house software ('iPDF').[42] Briefly, data were corrected for background, Compton scattering, and the atomic form factor. The Compton shift, detector efficiency, and incoherent fluorescence were also taken into account, before Fourier transformation according to

$$G(r) = \frac{2}{\pi}\int_0^\infty Q[S(Q) - 1]\sin(Qr)dQ$$

Here $Q[S(Q) - 1]$ represents the properly corrected and normalized intermediate structure factor and the r-grid used in real space had a spacing of 0.01 Å. Models were fitted to the PDF data using the EXPgui package. Here, the so-called small box approximation was used:

$$G(r) = \frac{1}{Nr}\sum_i\sum_{j\neq i}\left[\frac{b_i b_j}{\langle b\rangle^2}\delta(r - r_{ij})\right] - 4\pi r\rho_0$$

This implies that the first summation above only runs over the atoms within one unit cell as defined by the average crystallographic structure. This approximation makes data modeling tractable out to relatively large distances in real space. In the above equation, peaks in the PDF are weighted by the scattering power of each atomic species (b_i and b_j) divided by the average scattering power for the total unit cell contents. The detector was placed close to the sample such that a momentum transfer of 30 $Å^{-1}$ was reached at high angles. The raw 2D images were corrected for detector efficiency and radially integrated using Fit2D.[43] Energy calibration was provided by measuring a NIST CeO_2 standard. The sample was contained in a quartz capillary, and the background from an empty capillary was subtracted from the data set.

Recovered samples from the tetragonal and orthorhombic Hf_3N_4 preparations were analyzed by energy dispersive X-ray spectroscopy (ThermoFisher Ultradry detector with Noran System 7 acquisition system mounted on a Philips XL30-ESEM) and exhibited nitrogen

contents consistent with the initial composition, but these samples were exposed to air during their introduction into the scanning electron microscope, and a significant oxygen signal was also observed. This was assumed to be due to surface oxidation. Nanocrystalline Hf_3N_4 samples that were handled briefly in air before combustion analysis contained a significantly reduced amount of nitrogen, and so fast surface oxidation of the crystallized samples is also likely. Hence evidence of the compositions of these materials was taken from the Raman spectra and compressibilities relative to the isostructural oxides. The Raman spectra were recorded in a backscattering geometry on a Jobin-Yvon Labram spectrometer with a low-frequency cutoff at 100 cm^{-1} and an exciting laser line with λ = 633 nm. The laser was focused inside the DAC to a size of 2 μm with a ×20 magnification microscope objective and the power was kept at 5 mW.

■ AUTHOR INFORMATION

Corresponding Author

salamat@physics.harvard.edu; a.l.hector@soton.ac.uk; p.f.mcmillan@ucl.ac.uk

Notes

The authors declare no competing financial interest.

■ ACKNOWLEDGMENTS

The authors thank the European Synchrotron Radiation Facility for access to ID27 (CH-3515), ID15, and SNBL and H. Mueller for assistance with glovebox and chemistry facilities. B.M.G. is supported by EPSRC via a doctoral training grant studentship. Thanks to SAFC-HiTech for a gift of $Hf(NEtMe)_4$. AS thanks Sam Buttrick for assistance with image processing.

■ REFERENCES

(1) Inorganic Crystal Structure Database accessed via the EPSRC-funded Chemical Database Service at Daresbury: Fletcher, D. A.; McMeeking, R. F.; Parkin, D. *J. Chem. Inf. Comput. Sci.* **1996**, *36*, 746.

(2) Brese, N. E.; O'Keeffe, M. *Crystal Chemistry of Inorganic Nitrides: Complexes, Clusters and Crystal Chemistry*; Springer: Berlin/Heidelberg, 1992, pp 307−378.

(3) (a) Lengauer, W. *Handbook of Ceramic Hard Materials*; Riedel, R. Ed.; Wiley-VCH: Weinheim, 2000; Vol. *1*. (b) Mazumder, B.; Hector, A. L. *J. Mater. Chem.* **2009**, *19*, 4673.

(4) (a) Brauer, G.; Weidlein, J. R. *Angew. Chem.* **1965**, *77*, 218. (b) Brese, N. E.; O'Keeffe, M.; Rauch, P.; DiSalvo, F. J. *Acta Cryst. C* **1991**, *47*, 2291. (c) Henderson, S. J.; Hector, A. L. *J. Solid State Chem.* **2006**, *179*, 3518.

(5) (a) Guenther, E.; Jansen, M. *Mater. Res. Bull.* **2001**, *36*, 1399. (b) Jansen, M.; Guenther, E.; Letschert, H. P. German Patent 199 07 618.9, 1999.

(6) Hitoki, G.; Ishikawa, A.; Takata, T.; Kondo, J. N.; Hara, M.; Domen, K. *Chem. Lett.* **2002**, *31*, 736.

(7) (a) Ishikawa, A.; Takata, T.; Kondo, J. N.; Hara, M.; Domen, K. *J. Phys. Chem. B* **2004**, *108*, 11049. (b) Higashi, M.; Domen, K.; Abe, R. *Energy Env. Sci.* **2011**, *4*, 4138.

(8) Christensen, A. N. *Acta Chem. Scand. A* **1975**, *29*, 563.

(9) Salamat, A.; Hector, A. L.; Kroll, P.; McMillan, P. F. *Coord. Chem. Rev.* **2013**, *257*, 2063.

(10) Lerch, M.; Fuglein, E.; Wrba, J. *Z. Anorg. Allg. Chem.* **1996**, *622*, 367.

(11) (a) Zerr, A.; Miehe, G.; Serghiou, G.; Schwarz, M.; Kroke, E.; Riedel, R.; Fuess, H.; Kroll, P.; Boehler, R. *Nature* **1999**, *400*, 340. (b) Leinenweber, K.; O'Keeffe, M.; Somayazulu, M.; Hubert, H.; McMillan, P. F.; Wolf, G. H. *Chem.—Eur. J.* **1999**, *5*, 3076. (c) Serghiou, G.; Miehe, G.; Tschauner, O.; Zerr, A.; Boehler, R. *J. Chem. Phys.* **1999**, *111*, 4659. (d) Scotti, N.; Kockelmann, W.; Senker, J.; Traßel, S.; Jacobs, H. *Z. Anorg. Allg. Chem.* **1999**, *625*, 1435.

(12) Zerr, A.; Miehe, G.; Riedel, R. *Nat. Mater.* **2003**, *2*, 185.

(13) Dzivenko, D. A.; Zerr, A.; Boehler, R.; Riedel, R. *Solid State Commun.* **2006**, *139*, 255.

(14) Gregoryanz, E.; Sanloup, C.; Somayazulu, M.; Badro, J.; Fiquet, G.; Mao, H.-K.; Hemley, R. J. *Nat. Mater.* **2004**, *3*, 294.

(15) (a) Crowhurst, J. C.; Goncharov, A. F.; Sadigh, B.; Evans, C. L.; Morrall, P. G.; Ferreira, J. L.; Nelson, A. J. *Science* **2006**, *311*, 1275. (b) Young, A. F.; Sanloup, C.; Gregoryanz, E.; Scandolo, S.; Hemley, R. J.; Mao, H.-K. *Phys. Rev. Lett.* **2006**, *96*, 155501. (c) Crowhurst, J. C.; Goncharov, A. F.; Sadigh, B.; Zaug, J. M.; Aberg, D.; Meng, Y.; Prakapenka, V. B. *J. Mater. Res.* **2008**, *23*, 1.

(16) Ren, L.; Li, C.; Fan, F.; Guo, Q.; Liang, D.; Feng, Z.; S. Xiao, F.-S. *Chem.—Eur. J.* **2011**, *17*, 6162.

(17) Tsujimoto, Y.; Tassel1, C.; Hayashi, N.; Watanabe, T.; Kageyama, H.; Yoshimura, K.; Takano, M.; Ceretti, M.; Ritter, C.; Paulus, W. *Nature* **2007**, *450*, 1062.

(18) Yamanaka, S.; Kawaji, H.; Hotehama, K.; Ohashi, M. *Adv. Mater.* **1996**, *8*, 771.

(19) Hunter, S. M.; Mckay, D.; Smith, R. I.; Hargreaves, J. S. J.; Gregory, D. H. *Chem. Mater.* **2010**, *22*, 2898.

(20) Baxter, D. V.; Chisholm, M. H.; Gama, G. J.; DiStasi, V. F.; Hector, A. L.; Parkin, I. P. *Chem. Mater.* **1996**, *8*, 1222.

(21) (a) Jackson, A. W.; Shebanova, O.; Hector, A. L.; McMillan, P. F. *J. Solid State Chem.* **2006**, *179*, 1383. (b) Bailey, E.; Ray, N. M. T.; Hector, A. L.; Crozier, P.; Petuskey, W. T.; McMillan, P. F. *Materials* **2011**, *4*, 1747.

(22) Fix, R.; Gordon, R. G.; Hoffman, D. M. *Chem. Mater.* **1991**, *3*, 1138.

(23) Li, J.; Dzivenko, D.; Zerr, A.; Fasel, C.; Zhou, Y.; Riedel, R. *Z. Anorg. Allg. Chem.* **2005**, *631*, 1449.

(24) (a) Dzivenko, D. A.; Zerr, A.; Bulatov, V. K.; Miehe, G.; Li, J. W.; Thybusch, B.; Brotz, J.; Fuess, H.; Brey, G.; Riedel, R. *Adv. Mater.* **2007**, *19*, 1869. (b) Dzivenko, D. A.; Zerr, A.; Miehe, G.; Riedel, R. *J. Alloys Cmpds.* **2009**, *480*, 46.

(25) Kroll, P. *Phys. Rev. Lett.* **2003**, *90*, 125501.

(26) (a) Kroll, P.; Schroter, T.; Peters, M. *Angew. Chem., Int. Ed.* **2005**, *44*, 4249. (b) Kroll, P. *J. Phys.: Condens. Matter* **2004**, *16*, S1235.

(27) Qi, W. H.; Wang, M. P. *J. Nanopart. Res.* **2005**, *7*, 51.

(28) Morris, V. N.; Farrell, R. A.; Sexton, A. M.; Morris, M. A. *J. Phys. Conf. Ser.* **2006**, *26*, 119.

(29) (a) Jaffe, J. E.; Bachorz, R. A.; Gutowski, M. *Phys. Rev. B* **2005**, *72*, 144107. (b) Chen, X. J.; Struzhkin, V. V.; Kung, S.; Mao, H. K.; Hemley, R. J. *Phys. Rev. B* **2004**, *70*, 014501.

(30) Lowther, J. E. *Phys. Rev. B* **2005**, *72*, 172105.

(31) Piriou, B.; Arashi, H. *Bull. Mineral.* **1980**, *103*, 363.

(32) Ohtaka, O.; Fukui, H.; Kunisada, T.; Fujisawa, T.; Funakoshi, K.; Utsumi, W.; Irifune, T.; Kuroda, K.; Kikegawa, T. *J. Am. Ceram. Soc.* **2001**, *84*, 1369.

(33) Ohtaka, O.; Fukui, H.; Kunisada, T.; Fujisawa, T.; Kikegawa, T. *Phys. Rev. B* **2001**, *63*, 174108.

(34) Degreniers, S.; Lagarec, K. *Phys. Rev. B* **1999**, *59*, 8467.

(35) Haines, J.; Léger, J. M.; Hull, S.; Petitet, J. P.; Pereira, A. S.; Perottoni, C. A.; da Jornada, J. A. H. *J. Am. Ceram. Soc.* **1997**, *80*, 1910.

(36) Moura, C.; Carvalho, P.; Vaz, F.; Cunha, L.; Alves, E. *Thin Solid Films* **2006**, *515*, 1132.

(37) Mirgorodsky, A. P.; Quintard, P. E. *J. Am. Ceram. Soc.* **1999**, *82*, 3121.

(38) Curtis, C. E.; Doney, L. M.; Johnson, J. R. *J. Am. Ceram. Soc.* **1954**, *37*, 458.

(39) Tang, J.; Kai, M.; Kobayashi, Y.; Endo, S.; Shimomura, O.; Kikegawa, T.; Ashida, T. A High-Pressure High-Temperature X-Ray Study of Phase Relations and Polymorphism of HfO_2. In *Properties of Earth and Planetary Materials at High Pressure and Temperature*; Manghnani, M. H., Yagi, T., Eds.; American Geophysical Union: Washington, DC, 1998; pp 401−407.

(40) Schneider, S. B.; Baumann, D.; Salamat, A.; Schnick, W. *J. Appl. Phys.* **2012**, *111*, 093503.

(41) (a) Larson, A. C.; von Dreele, R. B. General Structure Analysis System (GSAS). *Los Alamos National Laboratory Report, LAUR 86-*

748; Los Alamos National Laboratory: Los Alamos, NM, 2000. (b) Toby, B. H. *J. Appl. Crystallogr.* **2001**, *34*, 210.
(42) The iPDF software was developed by one of the authors (S.A.J.K.). This software runs as a graphical user interface within Igor Pro and is available for noncommercial use on request (simon.kimber@esrf.fr).
(43) Hammersley, A. P.; Svensson, S. O.; Hanfland, M.; Fitchand, A. N.; Häusermann, D. *High Press. Res.* **1996**, *14*, 235.